2018

A Design Approach for Liquid Separators Applied to Household Refrigerators

Isabel Janke
Federal University of Santa Catarina, Brazil, isabel.janke@polo.ufsc.br

Alexsandro dos Santos Silveira
Federal University of Santa Catarina, Brazil, alex@polo.ufsc.br

Joel Boeng
melo@polo.ufsc.br

A Design Approach for Liquid Separators Applied to Household Refrigerators

Isabel JANKE, Alexsandro SILVEIRA, Cláudio MELO*

POLO - Research Laboratories for Emerging Technologies in Cooling and Thermophysics, Department of Mechanical Engineering, Federal University of Santa Catarina
Florianópolis, SC, Brazil
+55 48 32345691, melo@polo.ufsc.br

* Corresponding Author

ABSTRACT

The objective of this study was to develop a methodology for designing T-junction liquid-vapor separators for household refrigerators. The influence of the following independent parameters on the separator performance was studied: i) refrigerant mass flow rate, ii) inlet vapor quality, iii) phase-separation temperature, iv) critical droplet diameter and v) suction ratio. For modeling purposes, the T-junction was divided into three sub-models, namely: inlet, vapor and liquid branches. The inlet branch sub-model revealed that proper phase separation occurs with larger diameters as the refrigerant mass flow rate and vapor quality increase. The dimensions of the vapor branch are governed by the droplet diameter, vapor mass flow rate and phase-separation temperature, while the dimensions of the liquid branch are dictated by residence time, suction ratio and vapor quality. Additionally, a testing facility was designed and constructed to visualize the refrigerant flow through acrylic T-junctions mounted in a novel two-stage cycle architecture. A T-junction with an inlet branch diameter of 7 mm, a vertical branch diameter of 28 mm and total length of 58 mm was tested with compressor speeds ranging from 2000 to 3500 rpm and suction ratios from 10 to 45%. Photographs of the flow pattern through the separator were taken and used to explain the measured results.

1. INTRODUCTION

Economic and demographic development combined with the consequent growth of the food industry consolidated the market of domestic refrigerators and have massively stimulated the production of this product. By the year 2015, there were approximately 1.5 billion domestic refrigerators in operation worldwide (Coulomb and Dupont, 2015), and during 2009 alone, 80 million units were produced (Belman-Flores *et al*., 2015). In this context, concerns regarding environmental and energy demands have risen, leading to an extensive amount of research focused on new cycle architectures especially for appliances with two distinct refrigerated compartments.

The dual evaporator configurations with a single compressor, including serial, bypass and parallel cycles are all commercially available. There are, however, some disadvantages in their application, resulting mainly in performance losses. For instance, in the serial and bypass systems, the fresh food (FF) and the freezer (FZ) evaporators work almost at the same temperature level, leading to considerable performance losses. In the parallel cycle, the refrigerant trapped in the FZ evaporator must be periodically pumped-out, also leading to undesirable effects on system performance. On the other hand, multi-stage arrangements, such as dual-loop and two-stage cycles with two independent evaporation temperatures, offer the possibility of increasing the cooling capacity by separating the liquid and vapor phases before reaching the FZ evaporator.

Nevertheless, only a few studies have been focused on alternative cycle arrangements with phase separators for HC-600a household refrigerators. Yang *et al*. (2015), for example, conducted a simulation study considering four different two-stage cycles and concluded that the highest coefficient of performance (COP) is achieved when the evaporators

are connected in series and the compressors in parallel. On the other hand, phase separators, particularly T-junctions, have been extensively investigated by Milosevic (2010) and Tuo and Hrnjak (2014) for typical automotive air conditioning conditions using HFC-134a. Mello *et al.* (2016) experimentally investigated the HC-600a flow through separators with internal diameters of 6.35 and 12.7 mm under typical household refrigerators operating conditions. However, the authors did not examine in practical circumstances.

The ultimate goal of the present study was to develop a mathematical model to design phase separators for two-stage refrigerating systems, of the type schematically shown in Figure 1. In addition, a testing facility was designed and constructed to carry out experiments under different operating conditions. Lastly, visualization studies were conducted with the aim of correlating the refrigerant flow through the T-junction with the measured data.

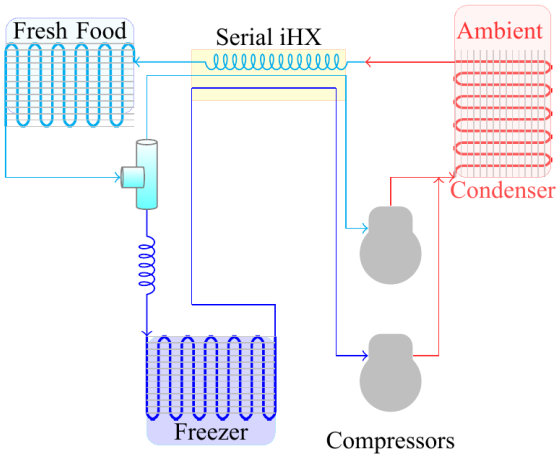

Figure 1: Serial two-stage cycle with phase-separator

2. EXPERIMENTAL WORK

A bottom-mount 220-liter frost-free refrigerator was used in the experiments. The original refrigeration cycle was deactivated and replaced with the two-stage circuit shown schematically in Figure 1. The liquid, medium and low pressure vapor lines were thermally insulated and positioned externally as illustrated in Figure 2. The system is comprised of a phase-separator, a tube-on-plate FF evaporator, a finned tube FZ evaporator, a wire-and-tube condenser, and two variable speed reciprocating compressors. Figure 2 also illustrates the positions where the temperature (±0.2°C) pressure (±0.01 bar) and power (±1.0 W) signals were recorded. The compartment temperatures were maintained at approximately 5°C and -18°C for the FF and FZ, respectively. The tests were carried out following the steady-state methodology proposed by Hermes *et al.* (2013), according to which electrical heaters are placed inside the compartments, while the compressors and the FZ-fan run continuously. The tests were performed in a climate controlled environment set to an ambient temperature of 25°C, with compressor speeds (N) of 2000, 2500, 3000 and 3500 rpm (both compressors always at the same speed) and suction ratios (φ) – fraction of time the product is operating in the fresh food mode – ranging from 10 to 45%. The refrigerant charge was previously determined and kept at 56 g in all tests.

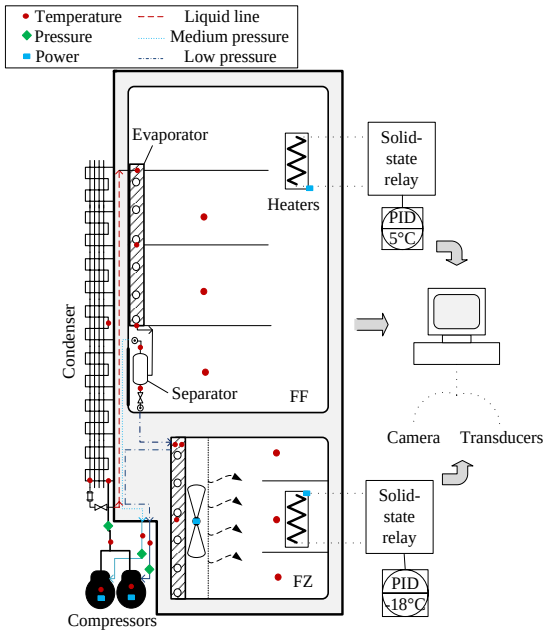

Figure 2: Sketch of testing facility

3. MATHEMATICAL MODEL

In this section, a mathematical model for designing T-type phase separators for HC-600a household refrigerating systems is briefly described. Three sub-models were developed, one for each of the branches illustrated in Figure 3a. The inlet branch sub-model is based on the criterion for stratified flow and the vapor branch on the settling theory. The liquid branch sub-model considers the residence time (t_R) of the liquid column and its degasification.

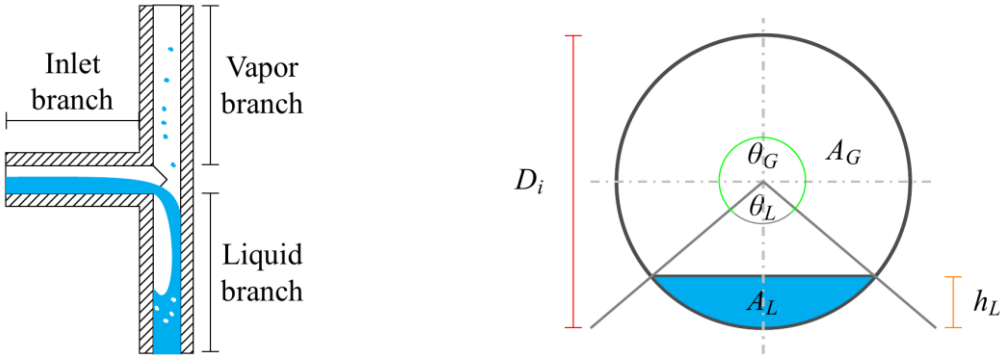

(a) T-junction phase separator and its three branches

(b) Inlet tube cross-section under fully stratified condition

Figure 3: Diagrams showing T-junction and inlet branch cross-sectional area

3.1 Inlet branch

Tuo and Hrnjak (2014) observed in their studies with HFC-134a that complete phase separation always occurs when the flow in the inlet branch follows a stratified pattern, characterized by a smooth liquid-vapor interface which occurs at very low mass fluxes, as shown in Figure 3b. However, two-phase flow pattern modelling correlations, specifically for HC-600a, are not readily available. Thus, the flow pattern map proposed by Kattan *et al.* (1998) was adopted in this work, not only due to its physical background, but also because it was satisfactorily validated with distinct refrigerants under various operating conditions. In this sub-model, the average refrigerant mass flow rate delivered by the two identical compressors to the separator is firstly calculated:

$$\dot{m} = \varphi V_k \left(\frac{N}{60}\eta_V \rho_{s1}\right) + (1-\varphi) V_k \left(\frac{N}{60}\eta_V \rho_{s2}\right) \tag{1}$$

where V_k stands for the volume of the compression chamber and η_v is the volumetric efficiency obtained from the manufacturer's catalogue. The vapor and liquid cross-sectional areas, A_G and A_L, are derived from the void fraction values provided by Rouhani and Axelsson's correlation (1970):

$$\alpha = \left(\frac{x}{\rho_G}\right)\left[(1+0.12(1-x))\left(\frac{x}{\rho_g}+\frac{(1-x)}{\rho_L}\right)+\frac{1.18(1-x)[g\sigma(\rho_L-\rho_G)]^{0.25}}{G{\rho_L}^{0.5}}\right]^{-1} \tag{2}$$

The variables θ_L and h_L are obtained by geometrical relationships taken from Figure 3b. The mass flux transition value between stratified and stratified-wavy flow is derived from the correlation proposed by Kattan *et al.* (1998) for smooth horizontal tubes:

$$G_{strat} = \left[226.3^2 \times \frac{\tilde{A}_L {\tilde{A}_G}^2 \rho_G(\rho_L-\rho_G)\mu_L g}{\pi^3 x^2(1-x)}\right]^{\frac{1}{3}} \tag{3}$$

where $\tilde{A}_L = A_L/D_i^2$ and $\tilde{A}_G = A_G/D_i^2$ are dimensionless cross-sectional areas. Therefore, if $G \leq G_{strat}$, D_i is a valid solution for the inlet branch. It should be noted that, for this particular application, diameters leading to a stratified-wavy flow pattern are also acceptable. The value for the mass flux transition value between stratified-wavy and annular/intermittent flow is given by:

$$G_{wavy} = \left[\frac{16{\tilde{A}_G}^3 g D_i \rho_L \rho_G}{\pi^2 x^2 \sqrt{1-(2\tilde{h}_L-1)^2}} \times \left[1+\frac{\pi^2}{25{\tilde{h}_L}^2}(1-x)^{G_1}\left[\left(\frac{Fr}{We}\right)_L\right]^{G_2}\right]\right]^{\frac{1}{2}} + 50 \tag{4}$$

where $\tilde{h}_L = h_L/D_i$ and, $G_1 = 0$ and $G_2 = 1.053$ considering adiabatic flow. The length of the inlet branch selected was 40 mm, as the refrigerant flow is likely to be separated. This selection was based on the results of Mello *et al.* (2016), who experimentally studied the flow of HC-600a within T-junctions and reported complete phase separation for similar mass flow rate conditions.

3.2 Vapor branch

The mathematical models used to describe the behavior of particles under relative motion are invariably based on the concept of the terminal velocity, which can be interpreted as the fluid velocity required to suspend a motionless particle (Seader *et al.*, 2011). The equations for the settling velocity of heavy-rigid ($\rho_L >> \rho_G$) and spherical (We < 6) (Villermaux and Bossa, 2009) particles vary according to the flow regime, as presented in Table 1. To identify the range in which the motion of the particle lies, the criterion *K* for a particle with diameter d_L proposed by McCabe *et al*. (1993) was applied:

$$K = d_L \left[g\rho_G \frac{(\rho_L - \rho_G)}{{\mu_G}^2} \right]^{\frac{1}{3}} \tag{5}$$

Table 1: Equations of u_t under different particle flow regimes

	Newton's Law	**Intermediate Law**	**Stokes' Law**
K	$68{,}9 \leq K \leq 2360$	$2.6 \leq K \leq 68.9$	≤ 2.6
$\mathbf{u_t}$	$1.75\sqrt{\frac{g d_L(\rho_L - \rho_G)}{\rho_G}}$	$0.153 g^{0.71} {d_L}^{1.14} \frac{(\rho_L - \rho_G)^{0.71}}{{\rho_G}^{0.29} {\mu_G}^{0.43}}$	$\frac{{g d_L}^2(\rho_L - \rho_G)}{18\mu_G}$

Having determined the mass flow rate, the suction ratio and assuming a value for the vapor branch inner diameter, D_G, the upward gas velocity can be calculated and compared to the terminal velocity. If $u_G < u_t$ the droplet will settle and, therefore, it will not be entrained towards the internal heat exchanger. As a result, D_G is a suitable diameter for this branch. According to Milosevic (2010), an estimate of the vertical vapor section minimum length is obtained as follows, even though this correlation was derived for designing horizontal separators.

$$L_G = \frac{4\dot{V}_{G,out}}{\pi u_t D_G} \tag{6}$$

3.3 Liquid branch

The presence of a liquid seal within the separator is required to prevent vapor flowing towards the FZ evaporator, compromising its performance. A quasi-steady approach for the prediction was thus developed based on the fundamental mass conservation law:

$$\frac{dm_L}{dt} = \dot{m}_{L_{in}} - \dot{m}_{L_{out}} = (1 - x)\dot{m} - (1 - \varphi)\dot{m} = (\varphi - x)\dot{m} \tag{7}$$

The liquid accumulated is $m_L = \rho_L V_L = \rho_L A L_L$. Substituting this value into Equation 7, considering ρ_L as a constant, and $D_L = D_G$, the result of the integration along the switching period (t_{sw}) gives:

$$L_L = \frac{4\,\dot{m}(\varphi - x)}{\rho_L \pi {D_G}^2} t_{sw} \tag{8}$$

The residence time, $t_R = V/\dot{V}_{L,out}$, governs the liquid degasification process, since it must be higher than the time required for a bubble to reach the free surface. It has been generally assumed that the downward movement of a heavy particle and the upward movement of a light particle in liquids are hydrodynamically similar. Nevertheless, several studies have cast doubts on this hypothesis in terms of the differences in the drag coefficients relationships and particle trajectory (Karamanev and Nikolov, 1992; Karamanev *et al*., 1996; Karamanev, 2001). The aforementioned reports on experimental investigations presented and discussed the use of the equation for the drag coefficient of rising spheres as a function of the Archimedes number $Ar = g {d_b}^3 (\rho_L - \rho_G)\rho_L {\mu_L}^{-2}$. Having determined L_L and $u_{t,b}$ (Equation 10), the degasification time can be calculated and compared to t_R.

$$C_D = \begin{cases} \frac{432}{\mathrm{Ar}}\left(1 + 0{,}0470\mathrm{Ar}^{\frac{2}{3}}\right) + \frac{0{,}517}{1+154\mathrm{Ar}^{\frac{-1}{3}}}, & \text{for Ar} < 13000 \\ 0.95, & \text{for Ar} > 13000 \end{cases} \quad (9)$$

$$u_{t,b} = \sqrt{\frac{4gd_b(\rho_L - \rho_G)}{3\rho_G C_D}} \quad (10)$$

4. RESULTS

The goals of this section are mainly to verify whether the proposed design methodology is appropriate to provide proper phase-separation and to investigate the effect of the flow in the separator on the compartments cooling capacity. The visualization exercise addressed the achievement of both objectives. The model analysis theoretically discusses the impact of the system operating conditions on the separator dimensions, while the experimental results address considerations regarding system performance for a selected geometry.

4.1 Model Results

Figure 4 shows the minimum diameter required for the inlet branch for varying compressor speed and vapor quality, at a phase-separation temperature of -10°C. It is worth noting that the diameter increases with increasing mass flow rate (compressor speed) and inlet quality. This is mainly due to the intense hydrodynamic interactions at the vapor-liquid interface, which requires larger diameters to maintain a stratified/stratified-wavy flow pattern. Figure 5 illustrates the effect of φ and N on the minimum vapor branch diameter for droplets ranging from 200 to 600 µm. As expected, this diameter varies with the size of the smallest droplet separated from the vapor flow, the compressor speed and the suction ratio. This is because the vapor mass flow rate and thus the vapor velocity – which has to be kept below certain limits to avoid liquid entrainment – are governed by the φ and N values. Figure 6 shows that smaller droplets and higher φ require longer vapor branch lengths for liquid disengagement.

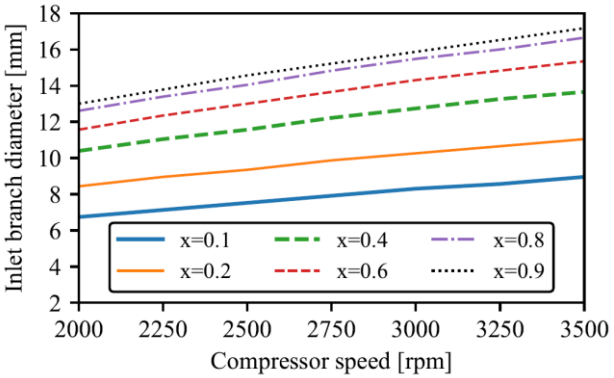

Figure 4: Minimum D_i versus N and x at T_{sep} = -10°C

Figure 7 shows the behavior of the liquid build-up at φ = 20% and 40% for various liquid branch diameters – assumed to be equal to the vapor diameter for practical purposes – a bubble diameter of 1 mm and switching period of 10 s. Clearly, a liquid column only appears within the separator when enough liquid is provided to this component. Hence, the presence of a liquid column will only occur when x is lower than φ, as inferred from Equation 8 and illustrated in Figure 7. Once the bubbles become too small (≈ 0.3 mm), the terminal velocity of the rising bubble decreases to a point where the bubble is dragged towards the FZ capillary. This implies that t_R is too short, indicating that the values of x are too close to φ or the liquid branch diameters are too narrow.

Figure 8 shows the minimum diameter and length required for the vapor branch for different particle sizes and two distinct phase-separation temperatures, T_{sep} = -10°C and T_{sep} = -15°C. At -15°C, when the droplets are smaller than 500 µm, the flow is governed by Stokes' Law (see Table 1) due to low ρ_G values, and phase-separation only occurs with wider diameters and low vapor velocity. As the droplets become larger, the flow regime changes to intermediate, u_t increases and phase-separation occurs more easily.

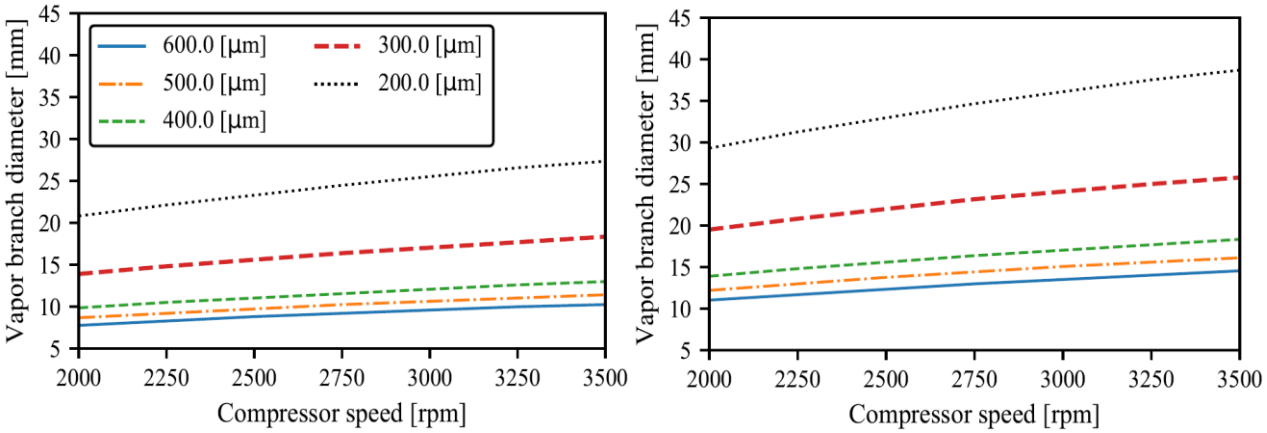

(a) φ = 20% **(b)** φ = 40%

Figure 5: Minimum vapor branch diameter versus N, d_L and φ at T_{sep} = -10°C

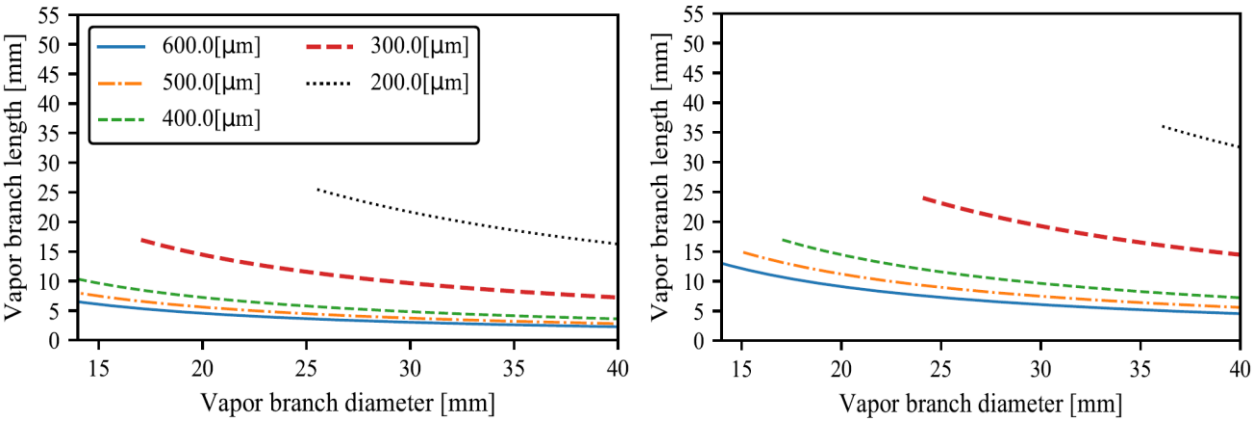

(a) φ = 20% **(b)** φ = 40%

Figure 6: Diameter and length of the vapor branch at 3000 rpm and T_{sep} = -10°C versus d_L and φ

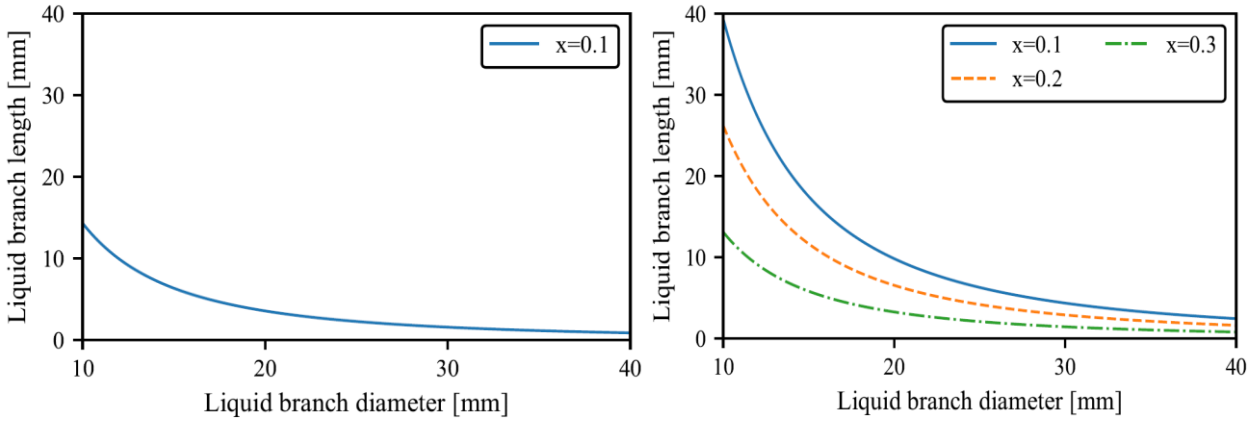

(a) φ = 20% **(b)** φ = 40%

Figure 7: Length of the liquid branch at 3000 rpm and T_{sep} = -10°C, d_b = 1 mm and t_{sw} = 10 s versus φ and x

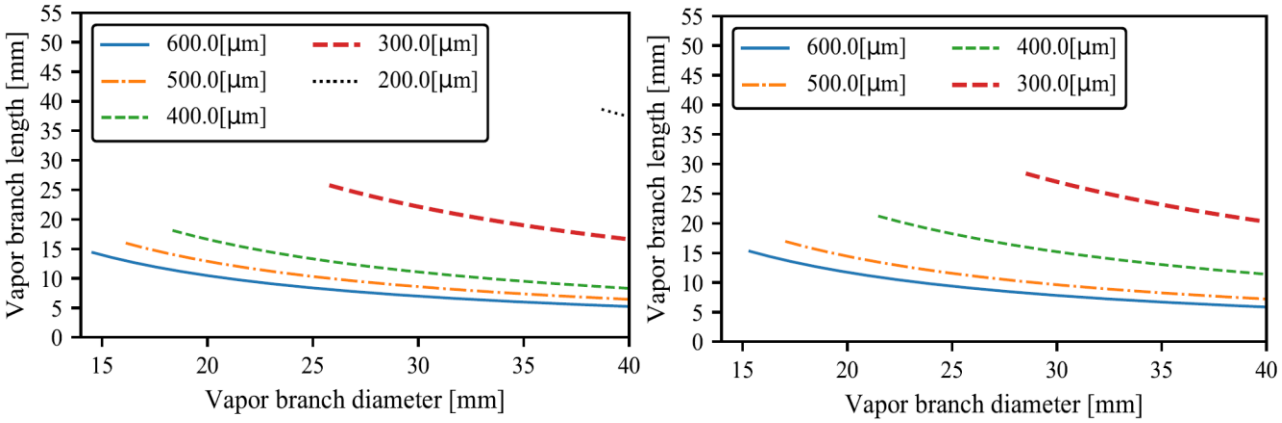

(a) T_{sep} = -10°C **(b)** T_{sep} = -15°C

Figure 8: Diameter and length of the vapor branch at 3500 rpm and φ = 40% versus d_L and T_{sep}

4.2 Experimental Results

Based on the model results, an acrylic T-type separator with D_i = 7 mm, D_G = 28 mm, L_G = 29 mm and L_L = 29 mm was manufactured and assembled in the testing apparatus to properly separate droplets up to 300 µm and bubbles greater than 1 mm in diameter at an evaporation temperature of -15°C. Figures 9a and 9b show photographs of the refrigerant flow through the separator branches at φ = 10% and φ = 40%, respectively.

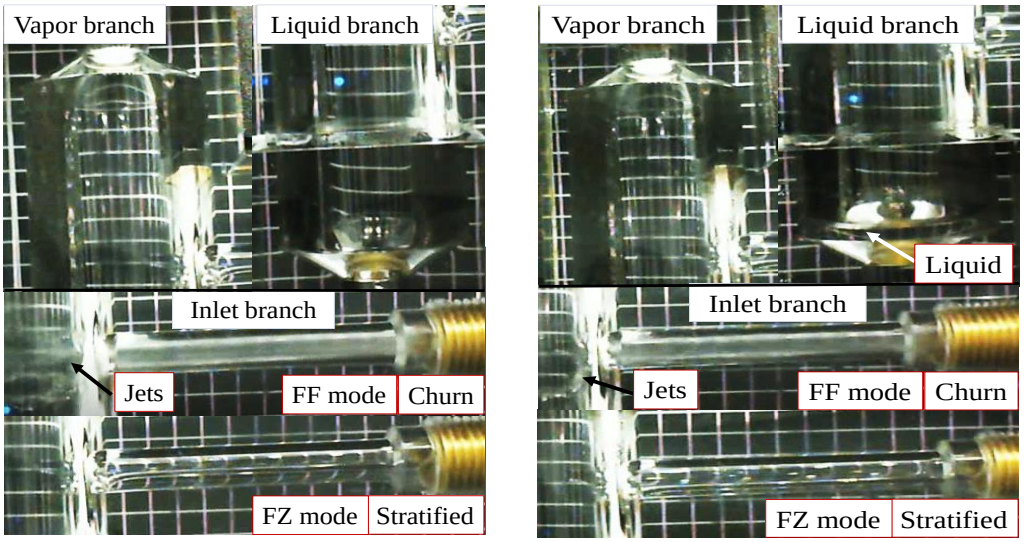

(a) φ = 10% **(b)** φ = 40%

Figure 9: Separator branches at 3500 rpm and φ = 10 and 40%

The photographs of the separator show that the flow pattern in the inlet branch changes from stratified to churn whenever the system is operating in the fresh food mode – when the instantaneous mass flow rate is higher – leading to liquid jets, which tend to divert in both upward and downward directions. As predicted by the model, increasing the vapor mass flow rate requires larger inlet diameters to ensure the stratified condition and thus, the diameter of 7 mm was not large enough to maintain this pattern at all times. However, stratified flow periods are inversely proportional to φ, due to longer periods of FZ mode at lower φ values and therefore, the stratified flow occurs during the majority of time. It should also be noted that the model has successfully designed the vapor branch, as no droplets were observed at the vapor outlet, even after the incoming liquid jets and low separation temperatures. Also, even though the vapor quality could not be precisely measured, the model has correctly predicted that low φ values provide no liquid seal, while at φ = 40% a liquid column of approximately 5 mm is observed. Figure 10 illustrates the behavior of the refrigerant flow as φ increases. It should be mentioned that all flow images in Figure 10 are of the system on the FZ mode

and, as previously explained, during this mode the flow in the inlet branch is always stratified. Figure 10 also shows that the liquid column rises and clear liquid degasification occurs, as large bubbles rise toward the interface, like predicted in the design stage.

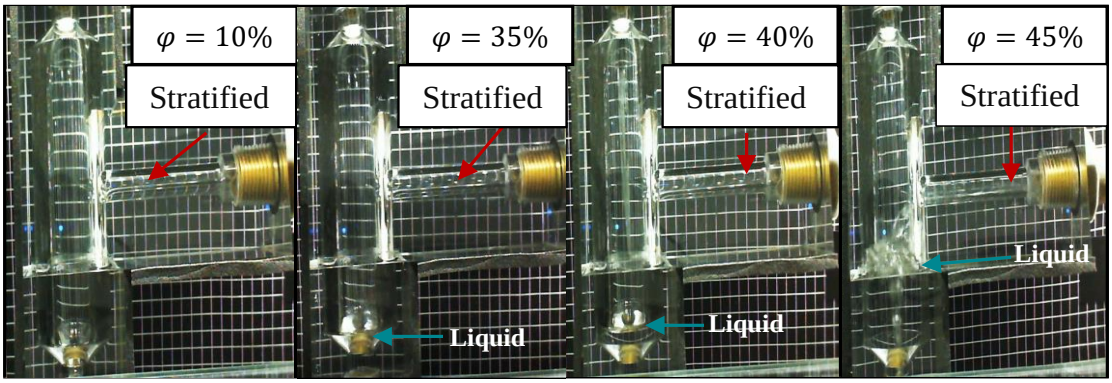

Figure 10: Liquid level in the separator at 3000 rpm and φ =10, 35, 40 and 45% on the FZ mode

The design methodology has demonstrated the ability of providing a geometry able to separate adequately the two phases. As a result, the system response in terms of cooling capacity when adopting these separator dimensions was analyzed. Figures 11a and 11b show the resulting cooling capacity of the fresh food and freezer compartments, respectively, at 3000 rpm. The evaporating temperature, superheating and internal compartment temperatures are also shown in these figures. It should be noted that the FF cooling capacity increases almost asymptotically as φ increases, accompanied by a similar behavior of the evaporating temperature. As expected, the lower the suction ratio the higher the compressor speed required to maintain the FF setpoint temperature will be. The negative superheating at the outlet of the flooded FF evaporator is mostly due to the pressure drop along the evaporator coil.

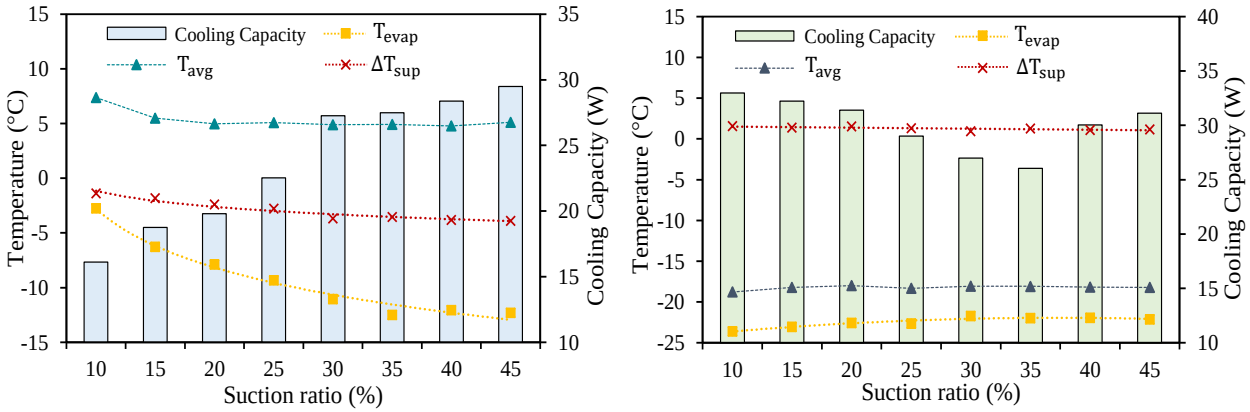

(a) Fresh food compartment **(b)** Freezer compartment

Figure 11: Cooling capacity as a function of φ at 3000 rpm

The FZ cooling capacity is substantially affected by the accumulation of liquid in the separator. At lower φ, the FF evaporating temperature is higher and so is the intermediate pressure. Thus, the refrigerant flows almost entirely to the FZ evaporator, with mostly vapor entering the FZ-capillary. At φ = 10% only a thin layer of liquid is observed at all speeds and there is no liquid build-up within the separator, as illustrated in Figure 10. As φ increases, a thin layer of liquid appears at φ = 35%. At this point, the liquid column is still intermittent and too short to allow complete degasification, and the FZ cooling capacity reaches a minimum value. This is mainly due to the opposite effects of the intermediate pressure and of the amount of liquid in the separator. At all speeds, the liquid begins to accumulate permanently at φ = 40%, its level rising gradually and simultaneously with the FZ cooling capacity, until complete degasification at φ = 45%. Lastly, as clearly shown in Figure 12, the combined cooling capacity (FF + FZ) is closely

related to the compressor speed and to the suction ratio, and thus to the accumulation of liquid in the separator. At lower φ values, the FF cooling capacity is too low and usually not enough to reach the FF setpoint temperature, as mentioned before. In such cases the FZ evaporator provides most of the combined cooling capacity. However, as φ increases, the rise of the FF cooling capacity balances the drop of the FZ cooling capacity until a certain point, where the FZ cooling capacity starts to increase due to the liquid seal in the separator. From this point on, the FF cooling capacity reaches an almost constant threshold value and the growth of the combined cooling capacity is provided mostly by the intensification of the two-phase heat transfer process in the FZ evaporator.

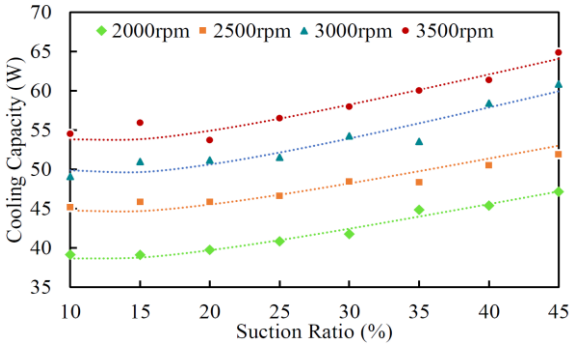

Figure 12: Cooling capacity versus N and φ

5. CONCLUSIONS

This paper describes a methodology to design phase-separators for HC-600a household refrigerators. The effect of this component over the thermodynamic performance of an innovative system architecture with two evaporators associated in series was also experimentally investigated. The design methodology is comprised of three sub-models, one for each branch of the separator: inlet, vapor and liquid. The visualization exercise revealed that the inlet flow is predominantly stratified, corroborating the model assumptions. The visualization study also verified that the flow to the internal heat exchanger is free of liquid droplets, validating the approach used for the vapor branch modeling. Additionally, it has been observed that liquid only starts to be accumulated in the separator at higher suction ratios, due to the lower inlet vapor qualities, as also predicted in the design stage. The design methodology provided a geometry that allowed the system to function appropriately during all tested conditions. It has also been shown that the combined cooling capacity increases with increasing suction ratio and compressor speed, with an optimal point at φ = 45%, as a result of the balancing between the cooling capacity of both compartments.

NOMENCLATURE

A	cross-sectional area	(m^2)	$\dot{m}$	mass flowrate	(kg/s)
Ã	dimensionless cross-sectional area	(-)	N	compressor speed	(rpm)
Ar	Archimedes number	(-)	T	temperature	(°C)
C_D	drag coefficient	(-)	t	time	(s)
COP	coefficient of performance	(-)	u	velocity	(m/s)
D	separator diameter	(m)	V	volume	(m^3)
d	particle diameter	(m)	$\dot{V}$	volumetric flowrate	(m^3/s)
FF	fresh food compartment	(-)	x	vapor quality	(-)
Fr	Froude number	(-)	We	Weber number	(-)
FZ	freezer compartment	(-)	α	void fraction	(-)
G	mass flux of liquid plus vapor	(Kg/m^2s)	η_V	volumetric efficiency	(-)
G_1, G_2	heat flux functions	(-)	θ	angle	(rad)
g	acceleration of gravity	(m/ s^2)	μ	dynamic viscosity	(Pa.s)
h̃	dimensionless height	(-)	ρ	density	(kg/m^3)
iHX	internal heat exchanger	(-)	σ	surface tension	(N/m)
K	criterion for settling regime	(-)	φ	suction ratio	(%)
L	vertical separator length	(m)			

Subscript

avg	average	out	at the separator outlet
b	bubble	R	residence
evap	evaporation	s_i	refrigerant state at suction line of compressor i
an	FZ-fan	sep	separation
G	gas/vapor phase	sw	switching
i	inlet section	strat	stratified flow
in	at the separator inlet	sup	superheating
k	compressor	t	terminal
L	liquid phase	wavy	wavy flow

REFERENCES

Belman-Flores, J., Barroso-Maldonado, J., Rodríguez-Munoz, A., & Camacho-Vázquez, G. (2015). Enhancements in domestic refrigeration, approaching a sustainable refrigerator - a review. *Renewable and Sustainable Energy Reviews*, 955-968.

Coulomb, D., & Dupont, J.-L. (2015). The role of refrigeration in the global economy. In *29th informatory note on refrigeration technologies.* Paris, France: International Institute of Refrigeration/IIR.

Hermes, C. J., Melo, C., & Knabben, F. T. (2013). Alternative test method to assess the energy performance of frost-free refrigerating appliances. *Applied Thermal Engineering*, 1029-1034.

Karamanev, D. (2001). The study of free rise of buoyant spheres in gas reveals the universal behaviour of free rising rigid spheres in fluid in general. *Int. J. of Multiphase Flow*, 1479-1486.

Karamanev, D., Chavarie, C., & Mayer, R. (1996). Dynamics of the free rise of a light solid sphere in liquid. *AIChE J.*, 1789-1792.

Karamanev, D., & Nikolov, L. (1992). Free rising spheres do not obey Newton's law for free settling. *AIChE J.*, 1843-1846.

Kattan, N., Thome, J. R., & Favrat, D. (1998). Flow boiling in horizontal tubes: Part 1—development of a diabatic two-phase flow pattern map. *J. Heat Transfer*, 140-147.

McCabe, W. L., Smith, J. C., & Harriott, P. (1993). *Unit operations of chemical engineering*. New York: McGraw-Hill.

Mello, I., Melo, C., & Boeng, J. (2016). Um estudo sobre separadores de líquido para refrigeração doméstica. In *Vi congresso ibero-americano de ciências e técnicas do frio.* Coimbra, Portugal.

Milosevic, A. S. (2010). *Flash gas bypass concept utilizing low pressure refrigerants.*

Rouhani, Z., & Axelsson, E. (1970). Calculation of volume void fraction in the subcooled and quality region. *Int. J. Heat Mass Transfer*, 383-393.

Seader, J., Henley, E. J., & Roper, K. D. (2011). *Separation process principles*. EUA: John Wiley & Sons.

Tuo, H., & Hrnjak, P. (2014a). Enhancement of vapor-liquid separation in vertical impact T-junctions for vapor compression systems with flash gas bypass. *Int. J. of Refrigeration*, 43-50.

Tuo, H., & Hrnjak, P. (2014b). Vapor-liquid separation in a vertical impact T-junction for vapor compression systems with flash gas bypass. *Int. J. of Refrigeration*, 189-200.

Villermaux, E., & Bossa, B. (2009). Single-drop fragmentation determines size distribution of raindrops. *Nature Physics*, 697-702.

Yang, M., Jung, C. W., & Kang, Y. T. (2015). Development of high efficiency cycles for domestic refrigerator-freezer application. *Energy, 93*, 2258–2266.

ACKNOWLEDGMENTS

This study was supported by the EMBRAPII Program (POLO/UFSC EMBRAPII Unit - Emerging Technologies in Cooling and Thermophysics). We thank Mr. Bruno Verardi for assistance with the experiments. We would also like to express our gratitude to Embraco S.A. for financial and technical support.